A Temperature-Dependent State of Charge Estimation Method Including Hysteresis for Lithium-Ion Batteries in Hybrid Electric Vehicles

EUNSEOK CHOI[1] AND SEKCHIN CHANG[2]

[1]SK Holdings, Seongnam, South Korea
[2]Department of Electrical and Computer Engineering, University of Seoul, Seoul 02504, South Korea

Corresponding author: Sekchin Chang (schang213@uos.ac.kr)

ABSTRACT Currently, lithium-ion batteries are mainly used as central power components in electric vehicles. Usually, accurate battery cell modeling and state of charge estimation are required in order to effectively use the lithium-ion batteries in electrified vehicles. For an elaborate battery cell modeling on a wide temperature range, we select a temperature-dependent battery cell modeling approach, which relies on one resistance plus second-order resistance-capacitance equivalent circuit model. In order to corporate some temperature effects into the modeling, we derive the sixth-order polynomial functions using the curve fitting algorithm. The functions contribute to the accurate battery cell modeling on the wide temperature range. For a practical usage of the functions in real-time embedded systems, we propose an offset-based lookup table technique. In addition, we propose a novel hysteresis voltage unit model for more accurate parameter estimation of hysteresis voltages. This also leads to more accurate battery cell modeling. Based on the battery cell modeling, we propose a temperature-dependent estimation method for state of charge. This approach exploits the extended Kalman filter, which is suitable for nonlinear characteristics such as the hysteresis effect. Experimental evaluation exhibits that the proposed estimation method outperforms the conventional approaches in the wide temperature range.

INDEX TERMS Equivalent circuit model, hysteresis model, state of charge, extended Kalman filter, lithium-ion battery, electrified vehicle.

I. INTRODUCTION

Recently, most fuel economy regulations increasingly require the automotive industry to reduce the carbon dioxide (CO2) emission, which is considered one of the most hostile behaviors to natural environments. In order to satisfy the regulations, the automotive manufacturers have been looking for new solutions, which are mainly based on lithium-ion batteries. The batteries usually guarantee high energy density and long service life. In addition, the lithium-ion batteries provide a compact size, a lower self-discharge rate, and various types including rechargeable battery. Therefore, the

The associate editor coordinating the review of this manuscript and approving it for publication was Pietro Savazzi.

lithium-ion batteries are suitable for especially electrified vehicles. However, the batteries have a potential safety hazard since they may make explosions and fires if damaged or incorrectly charged due to car accidents or electricity chargers with communication errors, respectively.

A battery management system (BMS) must be employed in electrified vehicles in order to ensure safe, reliable and efficient operations of the lithium-ion batteries. The BMS technologies consist of battery state estimation, cell management, contactor control, battery monitoring, crash sensing, and cooling/heating control: The battery state estimation estimates internal properties (SoC, state of health, internal resistance, capacity, current and power prognosis) of the battery system. The properties can usually be

estimated using the cell parameter identification [26]. The cell management determines the best cell thermal strategy, which includes the cell balancing and the defective cell detection. The contactor control realizes the state machine to control the switch on and off. It also controls the pre-load process and defines intermediate steps for the contactor switching sequence, and reports back whether the switch state has been operated correctly according to the desired switching request. The battery monitoring checks common battery signals such as the cell voltage/temperature, battery voltage/temperature, and SoC against the pre-defined limits. If the battery signals are monitored outside the pre-defined limits, the corresponding reactions are executed to protect the battery system. The crash sensing monitors external crash signal, and performs the appropriate error reaction in electrified vehicles. The cooling/heating control manages the temperature of battery cells/modules for overheat prevention within the battery and battery operation under low temperature environment. The BMS measures the sensing values (such as cell voltage, temperature, and pack current) from various sensors. Using the measured values, the BMS monitors the battery conditions such as fault state or normal state. In order to maintain an accurate state monitoring, the BMS is required to precisely estimate the remaining state of charge (SoC) and state of health (SoH) of a battery [1], [2]. Most electrified vehicle manufactures require the SoC RMSE and the maximum SoC error to be less than 1% and 3%, respectively in a wide temperature range [24], [27], [28]. An elaborate battery-cell model is of utmost importance in the BMS in order to achieve such SoC estimation accuracy. Furthermore, a real-time operation is required in the BMS for the electrified vehicle, which indicates that the BMS must be implemented as a real-time embedded system especially in the electrified vehicle. For the real-time requirement, the battery-cell model usually performs its operations in a real-time micro-processor in order to predict the SoC. Therefore, the battery-cell model must satisfy the low complexity and the high estimation accuracy requirements for the practical usage of lithium-ion batteries in electrified vehicles [3].

The battery cell models are classified into the electro-chemical model [4], [5] and the equivalent circuit model (ECM). In order to design the electro-chemical model, the behaviors of electrodes and electrolyte must be analyzed in the lumped battery. This model provides a high estimation accuracy. However, the model is not suitable for a real-time system since a huge number of mathematical operations are required in order to optimize lots of unknown parameters.

For the low complexity requirement, the ECM is more widely adopted in most real-time systems. The most popular example of the ECM can be found in the literatures of [6]–[8]. In addition, some practical ECMs are based on the resistance-capacitance (RC) networks. Such ECM types include one resistance plus first-order RC [9], one resistance plus second-order RC [10]–[12], and one resistance plus third-order RC [13], [14]. For the lithium-ion

battery in the electrified vehicle, a temperature-dependent ECM is required. Especially, the temperature-dependent ECM has been utilized for lithium-ion batteries with an electrothermal-aging model [29] and lithium-ion battery charging management considering economic costs of electrical energy loss and battery degradation [30]. The design of the temperature-dependent model usually relies on the open circuit voltage (OCV) characteristic curve of the battery, which depends the SoC and the temperature. The OCV-SoC curve can be expressed using various mathematical functions including exponential model, polynomial fitting model, sum of sine functions model, and Gaussian model under different temperatures [15]. However, the direct use of the mathematical functions may hinder a real-time operation. This indicates that the direct use is not suitable for the BMS in the electrified vehicle.

In the lithium-ion battery, the hysteresis effect exists during a charging/discharging cycle. Due to the effect, a difference can be found in the OCV. The difference is affected by the history of the battery usage, ambient/cell temperature, and the activities of electrodes and electrolyte in the battery [16]. For some lithium-ion batteries such as LiFePo4, the SoC estimation error is amplified if the battery cell model does not include the hysteresis effect [17]–[19]. In order to reflect the hysteresis effect, the one-state hysteresis model was proposed [7]. The hysteresis model was also adopted in various estimation approaches for the lithium-ion battery [20]–[22]. However, the conventional hysteresis model [7] uses a constant value as the maximum hysteresis voltage. This leads to fail in satisfying the SoC estimation error requirements. Therefore, the conventional model is not suitable for lithium-ion battery in the electrified vehicle.

This paper addresses a temperature-dependent SoC estimation approach for lithium-ion batteries in hybrid electric vehicles. The estimation technique is available on the entire temperature range, which covers the range of -20°C to 60°C. For the coverage of the entire temperature range, we select the temperature-dependent ECM, which includes one resistance plus second-order RC. In order to corporate the temperature effects into the ECM, we derive the sixth-order polynomial functions from the polynomial fitting model [15]. The curve fitting algorithm is utilized in the derivation. For a practical usage of the mathematical functions in the real-time BMS, we propose an offset-based lookup table technique. In order to satisfy the SoC estimation error requirements, we also propose a novel hysteresis voltage unit model, where the maximum hysteresis voltage adaptively changes according to the SoC range. Finally, we propose the temperature-dependent SoC estimation method, which is based on the temperature-dependent ECM. In order to manage the nonlinear characteristics including the hysteresis effect, the SoC estimation approach exploits the extended Kalman filter (EKF) [31].

In the paper, the unique contributions can be summarized as follows:

- The offset-based lookup table technique for a practical usage of the mathematical functions in the real-time BMS
- The novel hysteresis voltage unit model in order to satisfy the SoC estimation error requirements
- The temperature-dependent SoC estimation method (which relies on the offset-based lookup table technique and the hysteresis voltage unit model) suitable for lithium-ion batteries in electrified vehicles

The proposed SoC estimation utilizes the novel offset-based lookup table technique for practical cell parameter identification. This allows the SoC estimation to be applied in real applications such as real-time battery management systems.

Experimental evaluation reveals the validity of the proposed SoC estimation technique. The experimental results show that the presented estimation method gives an excellent accuracy performance in the entire temperature range. The results also exhibit that the proposed approach is superior to the conventional methods in the accuracy performance especially on the entire temperature range. The experimental results also guarantee that the proposed method fully satisfies the SoC estimation error requirements in the entire temperature range. This indicates that the presented SoC estimation approach is very suitable for lithium-ion batteries in electrified vehicles. While the algorithm was verified for a hybrid electric vehicle application, it would likely perform similarly for an electric vehicle application.

The fractional order model (FCM) [25], which is based on the online parameter identification, offers higher accuracy in the terminal voltage prediction. This leads to the improved SoC accuracy. Therefore, the FCM can be considered a good candidate for the SoC estimation. However, the FCM requires some data acquisition time for the parameter identification stability. Therefore, the proposed offline parameter identification technique needs to be used until the initial parameter identification is stable. After the stability, we can adaptively utilize the FCM for the SoC estimation.

Recently, some future trends were described in the battery state estimation domain [33]. Especially, a hybrid electrochemical-thermal-neural-network model was proposed for co-estimation of lithium-ion battery state of charge and state of temperature [34].

II. TEMPERATURE-DEPENDENT ECM

Figure 1 illustrates the generalized temperature-dependent ECM for battery cell modeling [23]. In Figure 1, $U_{OC}(SoC, T)$ denotes the OCV, which depends the SoC and the temperature (T). In Figure 1, I and V_t denote the input current and the terminal voltage, respectively. As shown in Figure 1, the ECM includes n RC networks, each of which consists of R_i (resistor i) and C_i (capacitor i) in parallel ($i = 1, 2, \cdots, n$). In Figure 1, R_0 represents an internal resistance. For the cell modeling of the lithium-ion battery, the circuit elements of Figure 1 are modeled using the experimental data of the input current (I) and the terminal voltage (V_t). In Figure 1, the circuit elements
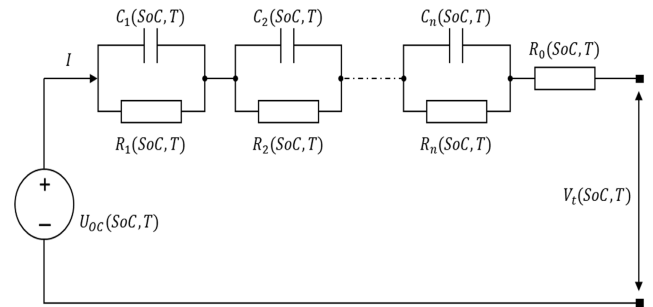

FIGURE 1. The generalized temperature-dependent ECM for battery cell modeling.

include $U_{OC}(SoC, T), R_o(SoC, T), R_1(SoC, T), C_1(SoC, T),$ $R_2(SoC, T), C_2(SoC, T), \ldots,$ and $R_n(SoC, T), C_n(SoC, T)$. In Figure 1, the number (n) of the RC networks also needs to be determined using the experimental data.

Figure 2 illustrates the experimental behaviors of the input current and the terminal voltage of the lithium-ion battery under the discharge pulse test at the temperature of 20°C. As shown in the figure, the lithium-ion battery discharges the current of −6.5 A for 3 minutes and has the rest period of 30 minutes. Figure 2 also shows that the voltage is accordingly discharged. As indicated in Figure 2, the SoC decreases as the voltage is discharged. Using the experimental curve of the voltage discharge, the circuit elements can be modeled. Figure 3 illustrates the voltage discharge curve of the lithium-ion battery under the discharge pulse test when the SoC decreases from 55% to 50% and the temperature is 20°C. Note that Figure 3 enlarges a part of the voltage discharge curve in Figure 2. In Figure 3, the internal resistance (R_0) can be modeled using the voltage drop. In addition, the n RC networks can be modeled using the RC transient response in Figure 3.
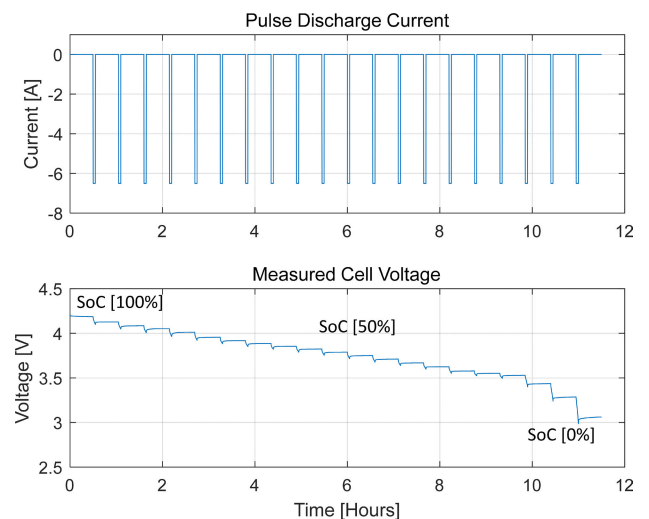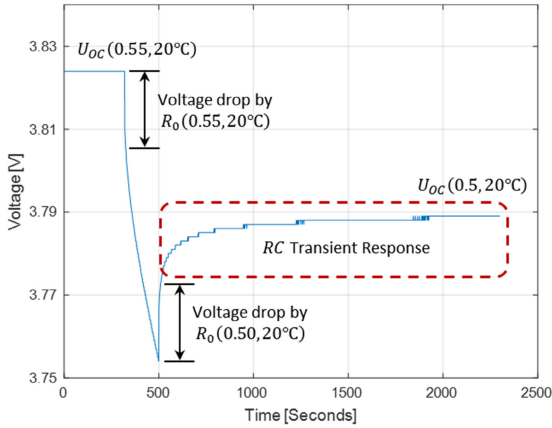

FIGURE 2. The experimental behaviors of the input current and the terminal voltage of the lithium-ion battery under the discharge pulse test @ 20°C.

FIGURE 3. The voltage discharge curve of the lithium-ion battery under the discharge pulse test @ SoC (55% to 50%) and 20°C.

In order to determine the number (n) of the RC networks, the *RC* transient response of Figure 3 is approximated to a curve fitting models. Figure 4 illustrates the curve fitting models for the *RC* transient response. Figure 4 shows the 2 curve fitting models: 1RC network and 2RC network. In Figure 4, the 1RC network and the 2RC network indicate the one resistance plus first-order RC [9] and the one resistance plus second-order RC [10]–[12], respectively.
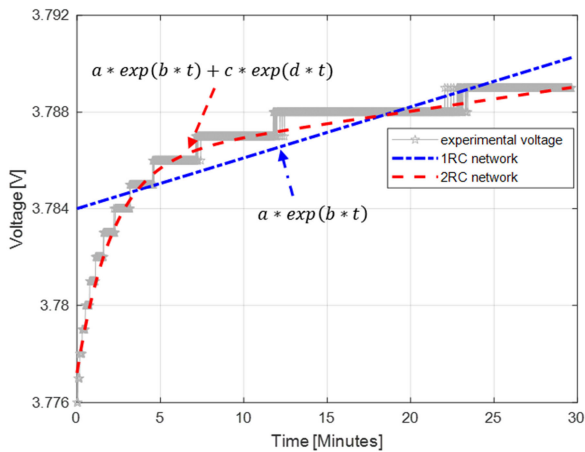
**FIGURE 4.** The curve fitting models for the RC transient response.

Table 1 exhibits the coefficients of the curve fitting models. Table 1 also shows the difference between the true *RC* transient response and each curve fitting model in terms of

TABLE 1. The coefficients and the RMSE values for the curve fitting models.

Network Form	a	b	c	d	RMSE
1RC Network	3.784	9.284e-07			0.0012680
2RC Network	3.786	4.481e-07	-0.008777	-0.007858	0.0003186

root mean squared error (RMSE). In Table 1, the unit of the RMSE is V. As indicated in Table 1, the 2RC network exhibits the lower RMSE value. Usually, more RC elements give better RMSE performance. In this paper, we select the 2RC network for the cell modeling of the lithium-ion battery as a tradeoff between model complexity and RMSE performance. Therefore, the number (*n*) of the RC networks is 2 in this paper for the cell modeling of the lithium-ion battery.
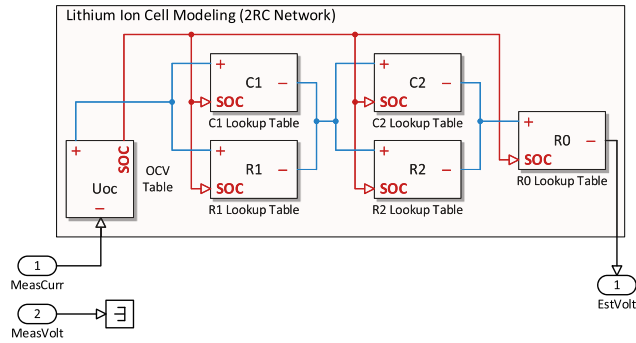
Figure 5 illustrates the selected temperature-dependent ECM for the cell modeling of the lithium-ion battery, which is based on the 2RC network. In Figure 5, the elements (R_0, R_1, C_1, R_2, and C_2) are modeled as the lookup table forms. The lookup tables are determined using the model-based parameter estimation by layered technique [13]. The real benefits of the 2RC network can be summarized as follows:
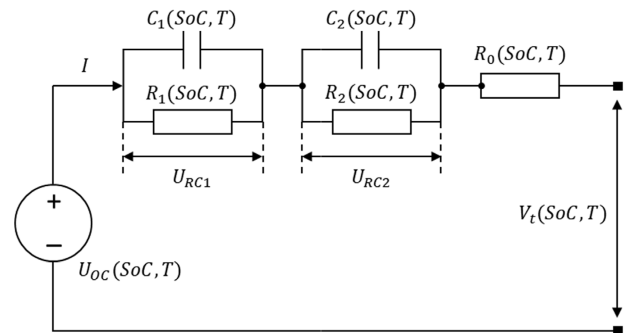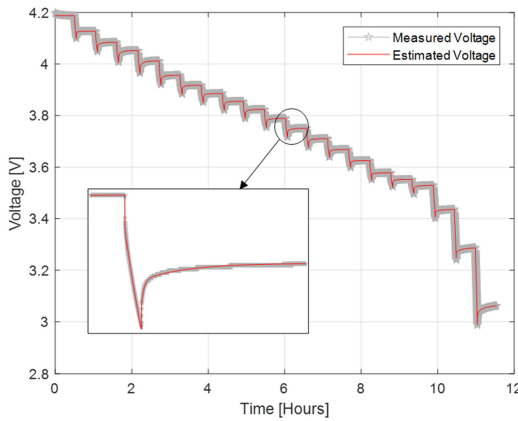

FIGURE 5. The selected temperature-dependent ECM for the cell modeling of the lithium-ion battery.

- As shown in Table 1, the 2RC network exhibits much better RMSE performance than the 1RC network.
- The 2RC network is suitable for real-time SoC estimation. More RC elements may give better RMSE performance. However, the number of the elements accordingly increases in the state vector of (7), which considerably increases the computational complexity of EKF for the SoC estimation.
- The 2 RC network satisfies the SoC estimation error requirements for lithium ion batteries in electrified vehicles, which is shown in Section IV.

Figure 6 illustrates the parameter estimation model for the determination of the lookup tables in the selected temperature-dependent ECM of Figure 5. In Figure 6, Meas-Curr and MeasVolt are the measured current and the measured voltage, respectively, which are measured using the discharge pulse test of the lithium-ion battery. In Figure 6, EstVolt denotes the estimated voltage, which is achieved using the temperature-dependent ECM of Figure 5. Using the nonlinear least squares function as an optimization method, the lookup tables of Figure 6 are determined, which minimize the difference between MeasVolt and EstVolt each SoC. Figure 7 exhibits a comparison of the measured cell voltage and the estimated cell voltage at the temperature of 20°C, which are achieved using the discharge pulse test and the selected temperature-dependent ECM, respectively.

FIGURE 6. The parameter estimation model for the determination of the lookup tables in the selected temperature-dependent ECM of Figure 5.

FIGURE 7. The voltage discharge curve of the lithium-ion battery under the discharge pulse test @ SoC (55% to 50%) and 20°C.

In order to corporate the temperature effects into the temperature-dependent ECM, the electrical behaviors of the cell modeling are given as follows:

$$
\begin{cases}
\dot{U}_{RC1} = -\dfrac{U_{RC1}}{R_1 C_1} + \dfrac{1}{C_1} I \\
\dot{U}_{RC2} = -\dfrac{U_{RC2}}{R_2 C_2} + \dfrac{1}{C_2} I \\
S\dot{o}C = \dfrac{1}{3600 C_q} I.
\end{cases}
\tag{1}
$$

$$
V_t(SoC, T) = U_{OC}(SoC, T) + U_{RC1} + U_{RC2} + R_o I. \tag{2}
$$

In (1) and (2), U_{RC1} and U_{RC2} denote the voltages of C_1 and C_2, respective in Figure 5, and C_q represents the battery capacity (unit: Ah). In (2), $U_{OC}(SoC, T)$ denotes the OCV at the specific SoC and temperature (T).

Figure 8 shows the measured OCV curve, which depends on SoC and temperature. To determine the OCV-SoC characteristics, we fully charge the cell at the rate of C/10. After 1-hour rest, we discharge the cell with 20 discharge pulses at the rate of C/10 until the complete discharge (the cell voltage of 2.7 V). There is 1-hour rest phase between the discharge pulses. From this discharge, we can achieve a discharge curve. Then, we charge the cell with 20 charge pulses at the rate of C/10 until the complete charge (the cell voltage of 4.2 V). There is 1-hour rest phase between the charge pulses.
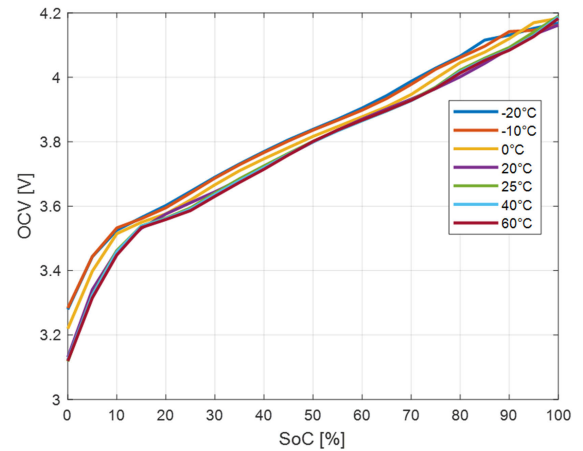
FIGURE 8. The OCV-SoC characteristics according to various temperatures.

From this charge, we can achieve a charge curve. Finally, we determine the OCV-SoC characteristics as the average of the discharge and the charge curves, which considers the hysteresis characteristics. The OCV-SoC characteristics of Figure 8 can be approximated to the curve fitting models. In this paper, we select the polynomial fitting models [15] as the curve fitting models. From the polynomial fitting models, we derive the sixth-order polynomial functions using the curve fitting algorithm. Therefore, the OCV-SoC behaviors of Figure 8 are approximated to the sixth-order polynomial functions, which are given in Table 2. In this Table, the parameter S denotes the SoC. As depicted in Table 2, we can achieve the sixth-order polynomial functions corresponding to the specific temperatures. Based on the sixth-order polynomial functions of Table 2, the temperature-dependent ECM can model the lithium-ion battery on a wide temperature range. However, the direct use of the polynomial functions hinders real-time operations in embedded systems since the management of many functions may cause an overload in memory resource and CPU. In order to satisfy the real-time requirement, we propose a lookup table approach, which is a modification of the technique [24]. The conventional lookup

TABLE 2. The sixth-order polynomial functions corresponding to the specific temperatures for the OCV-SoC behavior.

Temperature	Polynomial function: $U_{OC}(SoC, T) = f(S, T)$
-20°C	-21.79*S⁶ + 69.32*S⁵ - 87.02*S⁴ + 54.65*S³ - 17.92*S² + 3.638*S + 3.287
-10°C	-26.83*S⁶ + 83.86*S⁵ - 102.5*S⁴ + 62.08*S³ - 19.43*S² + 3.697*S + 3.291
0°C	-33.99*S⁶ + 107.7*S⁵ - 132.9*S⁴ + 80.8*S³ - 25.32*S² + 4.584*S + 3.223
20°C	-29.26*S⁶ + 98.24*S⁵ - 129*S⁴ + 84*S³ - 28.37*S² + 5.421*S + 3.131
25°C	-29*S⁶ + 97.67*S⁵ - 128.7*S⁴ + 84.18*S³ - 28.62*S² + 5.514*S + 3.117
40°C	-26.27*S⁶ + 90.19*S⁵ - 121*S⁴ + 80.35*S³ - 27.63*S² + 5.377*S + 3.122
60°C	-25.96*S⁶ + 89.52*S⁵ - 120.4*S⁴ + 80.04*S³ - 27.49*S² + 5.353*S +3.117

table technique [24] exhibits a computational complexity due to the linear interpolation, which is required in order to produce the OCV in the cases that the corresponding polynomial function for a specific temperature is not defined in the table. In order to avoid the complexity, we define a novel expression for $U_{OC}(SoC, T)$ as follows:

$$U_{OC}(SoC, T) = U_{OC}(SoC, 20^oC)$$
$$+ U_{Offset}(SoC, T) \times (T - 20^oC), \quad (3)$$

where $U_{OC}(SoC, 20^oC)$ is the sixth-order polynomial function at the temperature of 20°C, and $U_{Offset}(SoC, T)$ denotes the offset between $U_{OC}(SoC, 20^oC)$ and the measured OCV at the temperature of T and the same SoC. Based on the expression of (3), the proposed lookup table can simply produce the OCV at any temperature and SoC, which can significantly reduce the memory usage overhead and the CPU load. The proposed offset-based technique of (3) achieves some gains over the polynomial function method of Table 2 in the aspects of the memory usage overhead and the CPU load. If we use the 7 temperatures of Table 2 and 21 SoC values (0% to 100% with interval of 5%), the polynomial function method requires 21×7 memory array in the lookup table. In addition, the polynomial functions exhibit the OCV values ranging from 3.1 V to 4.2 V in Table 2. On the other hand, the offset method just requires 21×6 memory array in the lookup table since there is no offset OCV value in the case of 20°C in (3). This reduces the memory usage overhead. The offset method exhibits the offset OCV values ranging from -0.0051 V to 0.0055 V in (3). Compared with the OCV values of the polynomial function method, this enables faster interpolation, which reduces the CPU load.

III. PROPOSED HYSTERESIS VOLTAGE UNIT MODEL

Figure 9 exhibits a comparison of the OCV curves at the temperature of 20°C in the cases of charge and discharge under the same current value. As shown in Figure 9, the OCV curves are a little different each other. This phenomenon is called hysteresis. For some lithium-ion batteries such as LiFePo4, the SoC estimation error is amplified if the battery cell model does not include the hysteresis effect [17]–[19]. Therefore, the temperature-dependent ECM must employ a hysteresis voltage in order to reflect the hysteresis effect.

Figure 10 illustrates the temperature-dependent ECM with the hysteresis voltage (U_H) for the cell modeling of the lithium-ion battery. Using the one-state hysteresis model [7], the hysteresis voltage (U_H) can be expressed as follows:

$$\dot{U}_H = \exp\left(-\left|\frac{\gamma I}{3600 C_q}\right|\right) U_H + \left[1 - \exp\left(-\left|\frac{\gamma I}{3600 C_q}\right|\right)\right] M, \quad (4)$$

where γ and M denote a positive constant to tune the hysteresis rate and a maximum hysteresis voltage, respectively. The maximum hysteresis voltage is a positive constant and a negative constant in the cases of charge and discharge, respectively. In (4), the maximum hysteresis voltage (M) is
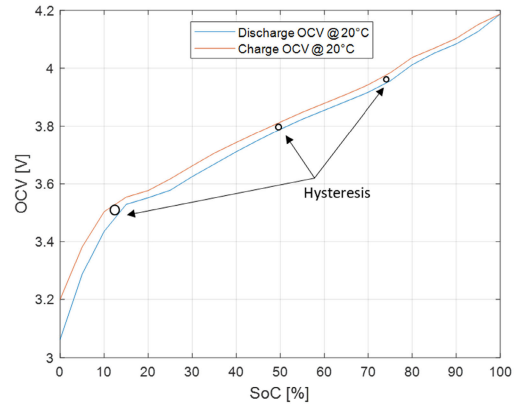

FIGURE 9. The OCV curves at the temperature of 20°C in the cases of charge and discharge under the same current value.
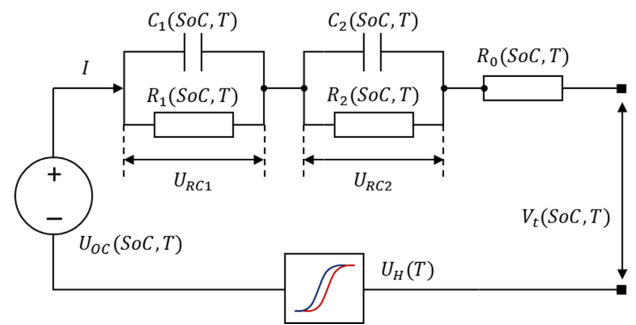

FIGURE 10. The temperature-dependent ECM with the hysteresis voltage for the cell modeling of the lithium-ion battery.

zero if the input current (I) is small enough. If the hysteresis voltage (U_H) is included in the temperature-dependent ECM, the expression of (2) can be extended as follows:

$$V_t(SoC, T) = U_{OC}(SoC, T) + U_{RC1} + U_{RC2} + U_H + R_o I. \quad (5)$$

As indicated in (5), the voltage $V_t(SoC, T)$ is affected by the hysteresis voltage (U_H). In the conventional hysteresis voltage unit model, the maximum hysteresis voltage (M) is assumed to be a constant for the entire range of the SoC [7], [20]–[22]. However, the hysteresis effect is different each SoC range as shown in Figure 9. Therefore, the conventional model does not satisfy the SoC estimation error requirements for the lithium-ion battery of the electrified vehicle.

In order to overcome the limitation of the conventional model, we propose the novel hysteresis voltage unit model, where the maximum hysteresis voltage (M) adaptively changes according to the SoC range. Figure 11 illustrates the proposed hysteresis voltage unit model for parameter estimation. In Figure 11, the lookup table (M_LUT) includes the separate maximum hysteresis each SoC range. In Figure 11, MeasVolt is the measured voltage. In Figure 11, EstVolt denotes the estimated voltage, which is calculated using (5). Using the nonlinear least squares function as an optimization
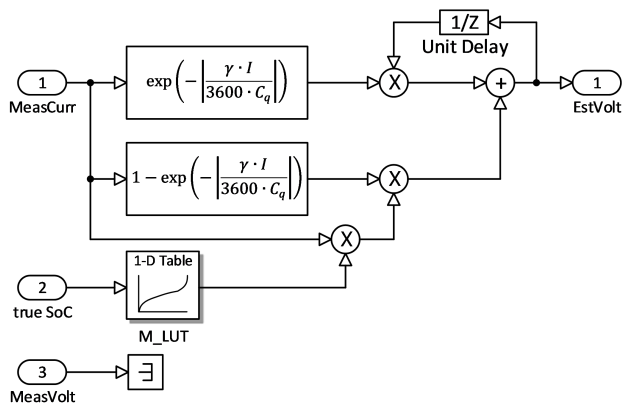
FIGURE 11. The proposed hysteresis voltage unit model for parameter estimation.

method, the parameters (γ and M) are determined, which minimizes the difference between MeasVolt and EstVolt each SoC range and each temperature.

Figure 12 exhibits a comparison of the measured cell voltage and the estimated voltages in the cases of only temperature-dependent ECM (Estimated Volt), temperature-dependent ECM with the conventional hysteresis model (Estimated Volt – M), and temperature-dependent ECM with the proposed hysteresis model (Estimated Volt – M LUT) at the temperature of 20°C. As shown in Figure 12, the estimated cell voltage of the proposed case is closer to the measured cell voltage than those of the other cases.
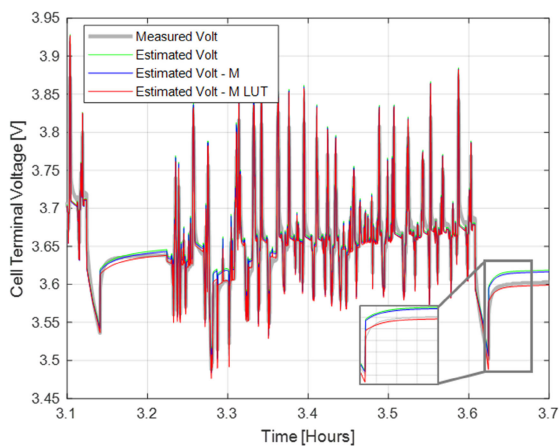

FIGURE 12. The comparison of the measures cell voltage and the estimated voltages in the cases of only temperature-dependent ECM (Estimated Volt), temperature-dependent ECM with the conventional hysteresis model (Estimated Volt – M), and temperature-dependent ECM with the proposed hysteresis model (Estimated Volt – M LUT) at the temperature of 20°C.

IV. PROPOSED TEMPERATURE-DEPENDENT SoC ESTIMATION

The temperature-dependent SoC estimation method is based on the temperature-dependent ECM of Figure 5, which also relies on the proposed hysteresis model. In the hysteresis

model, the hysteresis effect exhibits nonlinear dynamic characteristics. Therefore, the SoC estimation approach exploits the extended Kalman filter (EKF), which is very useful for nonlinear system analysis. For the SoC estimation based on the EKF, we define the state vector ($\mathbf{x}$) as follows: $\mathbf{x} = \begin{bmatrix} U_{RC1} & U_{RC2} & SoC \end{bmatrix}^T$. Using state vector ($\mathbf{x}$), the discrete-time state-space model of (1) can be expressed as follows:

$$\mathbf{x}_{k+1} = \begin{bmatrix} 1 - \dfrac{\Delta t}{R_1 C_1} & 0 & 0 \\ 0 & 1 - \dfrac{\Delta t}{R_2 C_2} & 0 \\ 0 & 0 & 1 \end{bmatrix} \mathbf{x}_k + \begin{bmatrix} \dfrac{\Delta t}{C_1} \\ \dfrac{\Delta t}{C_2} \\ \dfrac{\Delta t}{3600 C_q} \end{bmatrix} I_k, \quad (6)$$

where Δt denotes a sample time. If we consider the hysteresis voltage (U_H), the state vector ($\mathbf{x}$) can be extended as follows:

$$\mathbf{x} = \begin{bmatrix} U_{RC1} & U_{RC2} & U_H & SoC \end{bmatrix}^T. \quad (7)$$

In turn, the state-space model of (6) can be extended as follows:

$$\mathbf{x}_{k+1} = \begin{bmatrix} 1 - \dfrac{\Delta t}{R_1 C_1} & 0 & 0 & 0 \\ 0 & 1 - \dfrac{\Delta t}{R_2 C_2} & 0 & 0 \\ 0 & 0 & Hys(I_k) & 0 \\ 0 & 0 & 0 & 1 \end{bmatrix} \mathbf{x}_k$$
$$+ \begin{bmatrix} \dfrac{\Delta t}{C_1} & 0 \\ \dfrac{\Delta t}{C_2} & 0 \\ 0 & 1 - Hys(I_k) \\ \dfrac{\Delta t}{3600 C_q} & 0 \end{bmatrix} \begin{bmatrix} I_k \\ M \end{bmatrix}, \quad (8)$$

where $Hys(I_k)$ is defined as $\exp\left(-\left|\dfrac{\gamma I}{3600 C_q}\right|\right)$ in (4). For the SoC estimation, the EKF consists of prediction and update phases. In the prediction phase, the EKF performs the steps of (9) and (10) as follows:

$$\hat{\mathbf{x}}_k^- = \mathbf{F}_k \hat{\mathbf{x}}_{k-1} + \mathbf{B}_k \mathbf{u}_k, \quad (9)$$

$$\mathbf{P}_k^- = \mathbf{F}_k \mathbf{P}_{k-1} \mathbf{F}_k^T + \mathbf{Q}, \quad (10)$$

where

$$\mathbf{F}_k = \begin{bmatrix} 1 - \dfrac{\Delta t}{R_1 C_1} & 0 & 0 & 0 \\ 0 & 1 - \dfrac{\Delta t}{R_2 C_2} & 0 & 0 \\ 0 & 0 & Hys(I_k) & 0 \\ 0 & 0 & 0 & 1 \end{bmatrix},$$

$$\mathbf{B}_k = \begin{bmatrix} \dfrac{\Delta t}{C_1} & 0 \\ \dfrac{\Delta t}{C_2} & 0 \\ 0 & 1 - Hys(I_k) \\ \dfrac{\Delta t}{3600 C_q} & 0 \end{bmatrix}, \quad \text{and } \mathbf{u}_k = \begin{bmatrix} I_k \\ M \end{bmatrix}.$$

In (10), $\mathbf{Q}$ is defined as $\mathbf{Q} = E[\mathbf{w}_k \mathbf{w}_k^H]$, where $\mathbf{w}_k$ denotes a zero-mean Gaussian noise vector. For the operations in the update phase, the observation value (z_k) is defined as follows:

$$z_k = \mathbf{H}_k \hat{\mathbf{x}}_{k-1} + \mathbf{D}_k \mathbf{u}_k + v_k, \qquad (11)$$

where v_k denotes a measurement noise. From (5), the measured cell voltage (h_k) for the EKF is defined as follows:

$$h_k = f(SoC_k) + U_{RC1,k} + U_{RC2,k} + U_{H,k} + R_o I_k, \quad (12)$$

where $f(SoC_k)$ denotes the sixth-order function at the temperature of 20°C in Table 2. In (11), $\mathbf{H}_k$ and $\mathbf{D}_k$ are defined as follows:

$$\mathbf{H}_k = \left.\frac{\partial h_k}{\partial \mathbf{x}^T}\right|_{\hat{\mathbf{x}}_k} = \begin{bmatrix} 1 & 1 & 1 & \frac{\partial f(SoC_k)}{\partial SoC_k} \end{bmatrix},$$

$$\mathbf{D}_k = \left.\frac{\partial h_k}{\partial \mathbf{u}^T}\right|_{\mathbf{u}_k} = \begin{bmatrix} R_o & 0 \end{bmatrix}. \qquad (13)$$

In the update phase, the EKF also performs the steps of (14) to (17) as follows:

$$y_k = z_k - h_k. \qquad (14)$$

$$\mathbf{K}_k = \mathbf{P}_k^- \mathbf{H}_k^T \left(\mathbf{H}_k \mathbf{P}_k^- \mathbf{H}_k^T + R \right)^{-1}. \qquad (15)$$

$$\hat{\mathbf{x}}_k = \hat{\mathbf{x}}_k^- + \mathbf{K}_k y_k. \qquad (16)$$

$$\mathbf{P}_k = (\mathbf{I} - \mathbf{K}_k \mathbf{H}_k) \mathbf{P}_k^-. \qquad (17)$$

In (14), R is defined as follows: $R = E\left[|v_k|^2\right]$. In order to estimate the SoC accurately, the EKF repeats the prediction phase and the update phase.

V. EXPERIMENTAL EVALUATION

The experimental evaluation exhibits the effectiveness of the proposed temperature-dependent SoC estimation for lithium-ion batteries in electrified vehicles. We achieved the experimental results using Simulink (MATLAB-based Simulation tool). For this evaluation, we consider the following three models: only temperature-dependent ECM (only 2RC model), temperature-dependent ECM with the conventional hysteresis model (conventional model), and temperature-dependent ECM with the proposed hysteresis model (proposed model).

In order to extract the cell data, we varied the temperature range from 4.2 V (full charge) to 2.7 V (cut-off), and utilized a real-world driving profile. We used the urban dynamometer driving schedule (UDDS) [32] for the real-world driving profile. For the electrified vehicle test, we used the UDDS, which represents the city driving condition. In our test, the UDDS test sequence is separated by discharging pulses. There is a 5-minute rest period every test sequence. In the test, the SoC range is 0% to 100%. If the measured voltage is less than 2.7 V during the test sequence, the cycle is aborted. We used the following EV battery cell: SK Innovation, a lithium nickel manganese cobalt (NMC) oxide battery – NMC lithium ion battery, Ah rating: 6.5Ah, dimensions: 253mm × 172mm × 5.8mm (width, height, thickness), nominal voltage: 3.7 V,

nominal resistance: 2.65 mΩ. In the experiment, the test equipment is described as follows:

- PNE solution battery cycler (PEBC05-100)
- voltage measurement accuracy: 0.05% F.S. (0~5V)
- current measurement accuracy: 0.1% (measurement scale)

Figures 13, 14, and 15 illustrate the time-domain measurements for UDDS cycles. In the time-domain measurements, Figure 13 shows the current measurement for one UDDS cycle. In Figure 13, we achieved the current profile using the method of [8]. The method is described as follows [8]: "*The rate profile was generated from a MATLAB ADVISOR simulation for a vehicle roughly twice the size of the Honda Insight.*" The battery was tested with a UDDS drive cycle current profile for a large hybrid electric vehicle as is done in [8]. Prior to performing the first cycle, the battery is discharged to about 70% SoC to ensure that the upper voltage limit (4.2 V) is not exceeded. While cyclers can typically regulate current to prevent exceeding the upper voltage limit during charging pulses, the cycler used here cannot do so. After each UDDS cycle, which is approximately charge neutral, the battery is discharged by about 8% SoC and the UDDS and discharge cycles are repeated until 0% SoC (2.7 V) is reached. Figure 14 exhibits a comparison of the measured cell voltage and the estimated cell voltage as a function of time for UDDS cycles at 25°C. Figure 15 shows a comparison of the measured cell voltage and the estimated cell voltage as a function of time for UDDS cycles at −20°C.
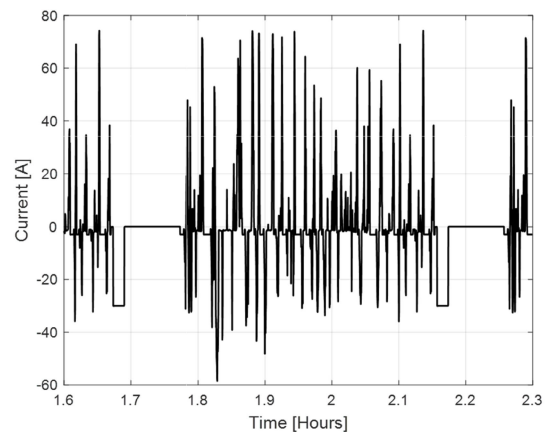

FIGURE 13. The current measurement for one UDDS cycle.

Table 3 shows a comparison of the three models at the entire temperature range (−20°C ~ 60°C) in terms of terminal voltage RMSE. In Table 3, the unit of the RMSE is mV. In Table 3, the RMSE is used as a performance measure to quantify the difference between the measured terminal voltage and the estimated terminal voltage. Table 3 reveals that the proposed model gives the best performance in the entire temperature range.

Table 4 exhibits a comparison of the three models at the entire temperature range in terms of SoC RMSE (unit: %). In Table 4, the RMSE is used as a performance measure
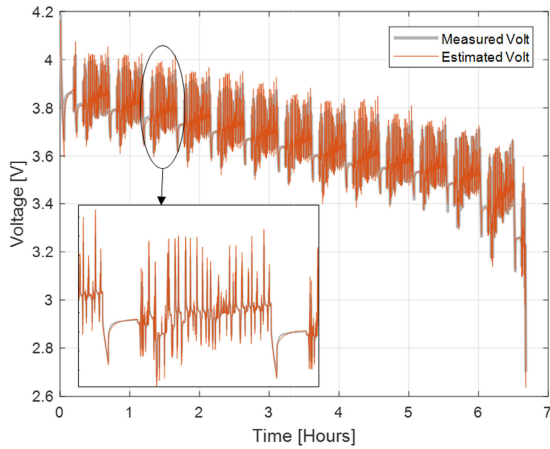
FIGURE 14. The comparison of the measured cell voltage and the estimated cell voltage as a function of time for UDDS cycles at 25°C.
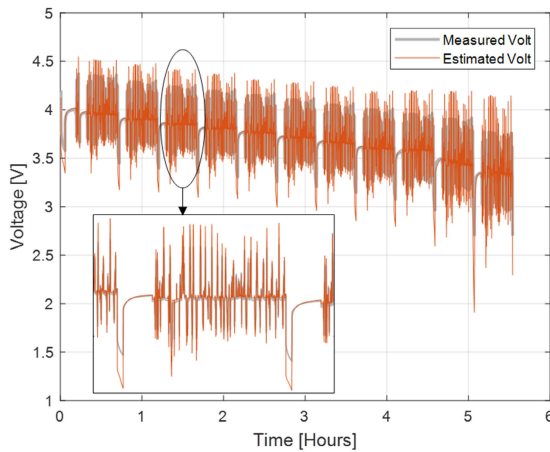
FIGURE 15. The comparison of the measured cell voltage and the estimated cell voltage as a function of time for UDDS cycles at −20°C.

TABLE 3. The comparison of the three models at the entire temperature range in terms of Terminal Voltage RMSE.

Temperature	-20°C	-10°C	0°C	20°C	25°C	40°C	60°C
Only 2RC Model	101.7	41.9	59.8	18.3	19.8	19.6	14.9
Conventional Model	82.9	31.9	54.9	18.2	19.7	16.6	13.9
Proposed Model	75.6	22.1	48.3	13.7	16.4	12.2	10.7

TABLE 4. The comparison of the three models at the entire temperature range in terms of SoC RMSE.

Temperature	-20°C	-10°C	0°C	20°C	25°C	40°C	60°C
Only 2RC Model	2.26	1.41	1.88	0.84	0.75	1.18	0.81
Conventional Model	1.39	0.75	0.60	0.64	0.58	0.43	0.29
Proposed Model	0.99	0.40	0.27	0.19	0.12	0.14	0.18

to quantify the difference between the true SoC and the estimated SoC. Table 4 indicates that the proposed model
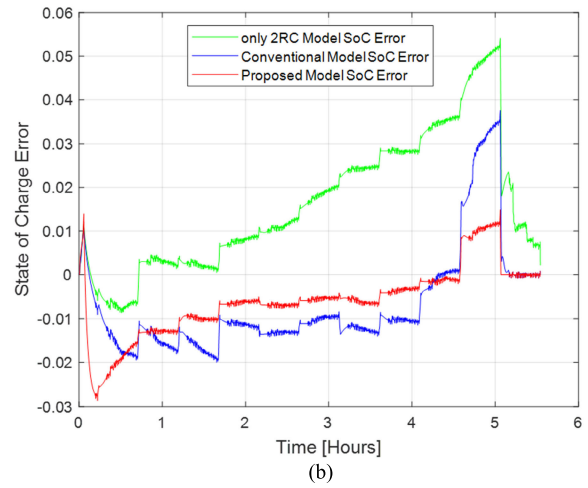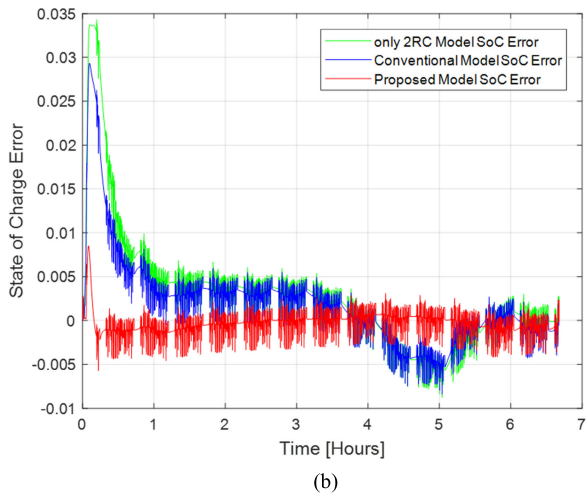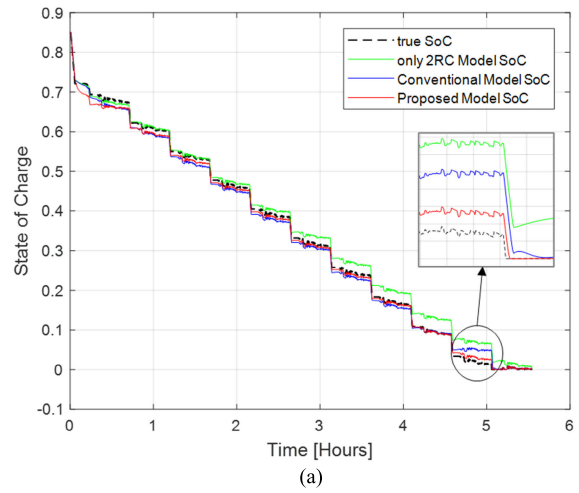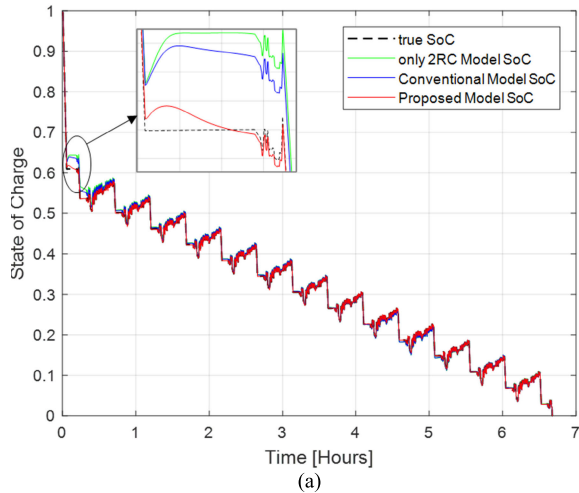
gives the lowest RMSE values in the entire temperature range. As shown in Table 4, the SoC RMSE of the proposed model is below 1% in the entire temperature range. This indicates that the proposed model satisfies the SoC RMSE requirement (below 1%) for lithium-ion batteries in electrified vehicles. Note that the other models do not satisfy the SoC RMSE requirement. Table 5 shows a comparison of the three models at the entire temperature range in terms of maximum absolute SoC error (unit: %). Table 5 reveals that the proposed model gives the best performance (in terms of maximum absolute SoC error) in the entire temperature range. As shown in Table 5, the maximum absolute SoC error of the proposed model is below 3% in the entire temperature range. This indicates that the proposed model also satisfies the requirement (below 3%) of the maximum absolute SoC error for lithium-ion batteries in electrified vehicles. Note that the other models do not satisfy the requirement of the maximum absolute SoC error.

TABLE 5. The comparison of the three models at the entire temperature range in terms of maximum absolute SoC error.

Temperature	-20°C	-10°C	0°C	20°C	25°C	40°C	60°C
Only 2RC Model	5.42	3.66	2.61	3.53	3.43	1.76	1.44
Conventional Model	3.76	3.08	1.94	2.86	2.93	1.18	1.09
Proposed Model	2.86	1.37	1.48	1.24	0.85	0.98	0.69

Figure 16(a) and (b) exhibit a comparison of the three models at the temperature of 25°C in terms of SoC curve and SoC error curve, respectively. For a cell voltage restriction, we apply a constant current (-50 A) during an initial time interval (about 180 s) in the experiment of Figure 16. Then, we apply the UDDS cycle. As indicated in Table 4, the only 2RC model and the proposed model exhibit the best SoC RMSE performance at the temperature of 25°C. Figure 16(a) exhibits that the estimated SoC curve of the proposed model is closer to the true SoC curve than those of the other models at the temperature of 25°C. Figure 16(b) shows that the proposed model converges to the error floor level more rapidly than the other models. In Figure 16(a), the rapid discharge is due to the constant current (-50 A) during the initial time interval (about 180 s).

Figure 17(a) and (b) shows a comparison of the three models at the temperature of −20°C in terms of SoC curve and SoC error curve, respectively. For a cell voltage restriction, we apply a constant current (−16.7 A) during an initial time interval (about 180 s) in the experiment of Figure 17. Then, we apply the UDDS cycle. As indicated in Table 5, all the models have the largest maximum absolute SoC errors at the temperature of −20°C. Figure 17(a) exhibits that the estimated SoC curve of the proposed model is closer to the true SoC curve than those of the other models at the temperature of −20°C. As indicated in Figure 17(b), the proposed model exhibits the best performance in terms of maximum absolute SoC error. In Figure 17(a), the rapid discharge is due to the

FIGURE 16. The comparison of the three models at the temperature of 25°C in terms of SoC curve and SoC error curve.

FIGURE 17. The comparison of the three models at the temperature of −20°C in terms of SoC curve and SoC error curve.

constant current (−16.7 A) during the initial time interval (about 180 s).
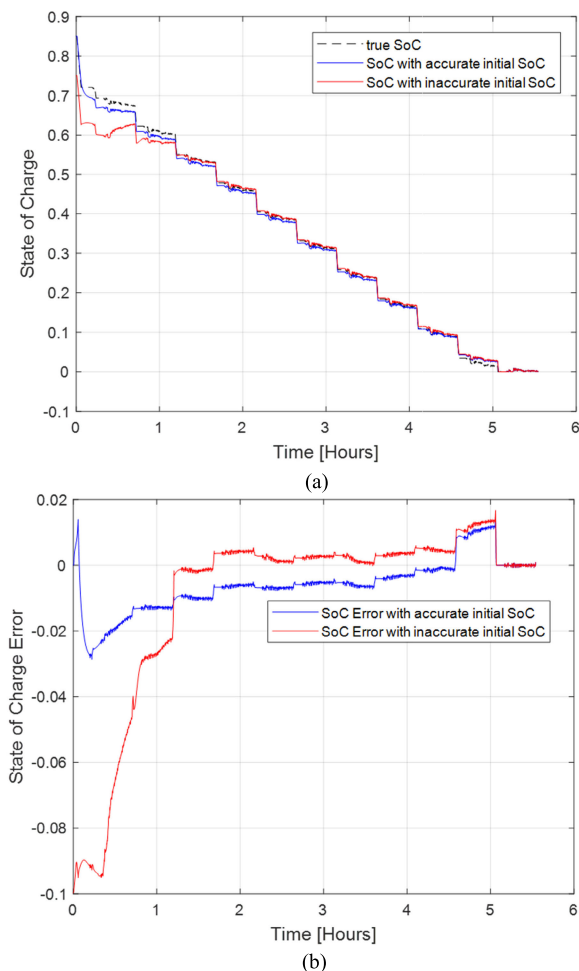
Table 6 exhibits a comparison of the cases of accurate initial SoC and inaccurate initial SoC for the proposed model at the entire temperature range in terms of SoC RMSE (unit: %). For the case of inaccurate initial SoC, the initial SoC includes the error of 10% in this experimental evaluation. Table 6 indicates that the proposed model renders larger SoC RMSE values in the entire temperature range due to the inaccurate initial SoC. However, the larger SoC errors will eventually vanish in the proposed model, which is verified in Figure 18.

TABLE 6. The comparison of the cases of accurate initial SoC and inaccurate initial SoC for the proposed model at the entire temperature range in terms of SoC RMSE.

Temperature	-20°C	-10°C	0°C	20°C	25°C	40°C	60°C
Accurate Initial SoC	0.99	0.40	0.27	0.19	0.12	0.14	0.18
Inaccurate Initial SoC	3.03	0.84	1.46	1.11	1.74	1.69	1.42

Figure 18(a) and (b) exhibit a comparison of the two cases (accurate initial SoC and inaccurate initial SoC) for the proposed model at the temperature of -20°C in terms of SoC curve and SoC error curve, respectively. As shown in Table 6, the proposed model gives the worst SoC RMSE performance at the temperature of -20°C in both cases. Figure 18(a) indicates that the estimated SoC of the inaccurate initial SoC case is more deviated from the true SoC than that of the accurate initial SoC case before 1 hour. However, the estimated SoC curves of both cases are almost identical to the true SoC after 5 hours in Figure 18(a). Similarly, Figure 18(b) indicates that the SoC error of the inaccurate initial SoC case is much larger than that of the accurate initial SoC before 1 hour. Like the case of Figure 18(a), the SoC errors of both initial SoC cases almost vanish after 5 hours in Figure 18(b). From the results of Figure 18(a) and (b), it is revealed that the estimated SoC will eventually converge to the true SoC in the proposed model even in the case that the initial SoC includes some error.

For lithium ion batteries in electrified vehicles, most electrified vehicle manufacturers require the SoC RMSE and the

FIGURE 18. The comparison of the two cases (accurate initial SoC and inaccurate initial SoC) for the proposed model at the temperature of −20°C in terms of SoC curve and SoC error curve.

maximum SoC error to be less than 1% and 3%, respectively in the entire temperature range. The experimental results verify that the proposed model fully satisfies the SoC estimation error requirements for lithium ion batteries in electrified vehicles. Furthermore, the proposed model allows the estimated SoC to eventually converge to the true SoC even with the inaccurate initial SoC.

VI. CONCLUSION
In this paper, we propose the temperature-dependent SoC estimation approach for lithium-ion batteries in electrified vehicles. The SoC estimation exploits a battery cell model of the lithium-ion battery. For the battery cell model, we select the temperature-dependent ECM, which consists of one resistance plus second-order RC. For the operation of the ECM on the entire temperature range (−20°C to 60°C), we derive the sixth-order polynomial functions, which belong to the polynomial fitting model [15]. We also present an offset-based lookup table technique, which allows a practical usage of the sixth-order polynomial functions in real-time embedded systems. In addition, we propose the novel hysteresis voltage unit model for the temperature-dependent ECM.

This allows the temperature-dependent SoC estimation method to satisfy the SoC estimation error requirements for lithium-ion batteries in electrified vehicles. We also propose the temperature-dependent SoC estimation method based on the EKF, which is very useful for nonlinear characteristics such as the hysteresis effect or the OCV-SoC curves. Using the discrete-time state-space model of the temperature-dependent ECM, we suggest the procedures of the EKF in the prediction phase and the update phase. The EKF procedures employ the operations of the temperature-dependent ECM. The EKF repeats the prediction phase and the update phase until the SoC is accurately estimated.

The experimental results exhibit that the proposed approach outperforms the conventional methods on the entire temperature range in terms of voltage RMSE, SoC RMSE and maximum absolute SoC error. The results also show that the proposed method fully satisfies the SoC estimation error requirements for lithium-ion batteries in electrified vehicles. Moreover, the experimental results verify that the proposed technique can eventually produce the accurate SoC estimate even with inaccurate initial SoC values. From the results, it is confirmed that the proposed SoC estimation approach is very suitable for lithium-ion batteries in electrified vehicles.

For the battery health prediction, we need to use addition model such as empirical exponential and polynomial model, and deep learning model. Therefore, we have to incorporate the additional model into the SoC estimation approach. As further work, we consider the SoC estimation method based on the additional model as well as the temperature-dependent ECM, which reflects the battery capacity degradation effect.

REFERENCES
[1] K. W. E. Cheng, B. P. Divakar, H. Wu, K. Ding, and H. F. Ho, "Battery-management system (BMS) and SoC development for electrical vehicles," *IEEE Trans. Veh. Technol.*, vol. 60, no. 1, pp. 76–88, Jan. 2011.

[2] H. Rahimi-Eichi, U. Ojha, F. Baronti, and M.-Y. Chow, "Battery management system: An overview of its application in the smart grid and electric vehicles," *IEEE Ind. Electron. Mag.*, vol. 7, no. 2, pp. 4–16, Jun. 2013.

[3] X. Hu, S. Li, and H. Peng, "A comparative study of equivalent circuit models for Li-ion batteries," *J. Power Sources*, vol. 198, pp. 359–367, Jan. 2012.

[4] A. P. Schmidt, M. Bitzer, Á. W. Imre, and L. Guzzella, "Experiment-driven electrochemical modeling and systematic parameterization for a lithium-ion battery cell," *J. Power Sources*, vol. 195, no. 15, pp. 5071–5080, Aug. 2010.

[5] T. Wang, K. J. Tseng, S. Yin, and X. Hu, "Development of a one-dimensional thermal-electrochemical model of lithium ion battery," in *Proc. IECON-39th Annu. Conf. IEEE Ind. Electron. Soc.*, Nov. 2013, pp. 6709–6714.

[6] G. L. Plett, "Extended Kalman filtering for battery management systems of LiPB-based HEV battery packs: Part 1. Background," *J. Power Sources*, vol. 134, no. 12, pp. 252–261, 2004.

[7] G. L. Plett, "Extended Kalman filtering for battery management systems of LiPB-based HEV battery packs: Part 2. Modeling and identification," *J. Power Sources*, vol. 134, no. 2, pp. 262–276, Aug. 2004.

[8] G. L. Plett, "Extended Kalman filtering for battery management systems of LiPB-based HEV battery packs: Part 3. State and parameter estimation," *J. Power Sources*, vol. 134, no. 2, pp. 277–292, 2004.

[9] C. Lin, X. Zhang, R. Xiong, and F. Zhou, "A novel approach to state of charge estimation using extended Kalman filtering for lithium-ion batteries in electric vehicles," in *Proc. IEEE Conf. Expo Transp. Electrific. Asia–Pacific (ITEC Asia–Pacific)*, Aug. 2014, pp. 1–6.

[10] Y. Hu and S. Yurkovich, "Linear parameter varying battery model identification using subspace methods," *J. Power Sources*, vol. 196, no. 5, pp. 2913–2923, Mar. 2011.

[11] W. Li, L. Liang, W. Liu, and X. Wu, "State of charge estimation of lithium-ion batteries using a discrete-time nonlinear observer," *IEEE Trans. Ind. Electron.*, vol. 64, no. 11, pp. 8557–8565, Nov. 2017.

[12] Q.-Z. Zhang, X.-Y. Wang, and H.-M. Yuan, "Estimation for SoC of Li-ion battery based on two-order RC temperature model," in *Proc. 13th IEEE Conf. Ind. Electron. Appl. (ICIEA)*, May 2018, pp. 2601–2606.

[13] R. Jackey, M. Saginaw, P. Sanghvi, and J. Gazzari, "Battery model parameter estimation using a layered technique: An example using a lithium iron phosphate cell," SAE Tech. Paper 2013-01-1547, 2013.

[14] R. Ahmed, J. Gazzarri, S. Onori, S. Habibi, R. Jackey, K. Rzemien, J. Tjong, and J. LeSage, "Model-based parameter identification of healthy and aged Li-ion batteries for electric vehicle applications," *SAE Int. J. Alternative Powertrains*, vol. 4, no. 2, pp. 233–247, Apr. 2015.

[15] R. Zhang, B. Xia, B. Li, L. Cao, Y. Lai, W. Zheng, H. Wang, W. Wang, and M. Wang, "A study on the open circuit voltage and state of charge characterization of high capacity lithium-ion battery under different temperature," *Energies*, vol. 11, no. 9, p. 2408, Sep. 2018.

[16] H. R. Eichi and M.-Y. Chow, "Modeling and analysis of battery hysteresis effects," in *Proc. IEEE Energy Convers. Congr. Expo. (ECCE)*, Sep. 2012, pp. 4479–4486.

[17] T. Kim, W. Qiao, and L. Qu, "Hysteresis modeling for model-based condition monitoring of lithium-ion batteries," in *Proc. IEEE Energy Convers. Congr. Expo. (ECCE)*, Sep. 2015, pp. 5068–5073.

[18] F. Baronti, W. Zamboni, N. Femia, R. Roncella, and R. Saletti, "Experimental analysis of open-circuit voltage hysteresis in lithium-iron-phosphate batteries," in *Proc. IECON-39th Annu. Conf. IEEE Ind. Electron. Soc.*, Nov. 2013, pp. 6728–6733.

[19] T. Huria, M. Ceraolo, J. Gazzarri, and R. Jackey, "Simplified extended Kalman filter observer for SoC estimation of commercial power-oriented LFP lithium battery cells," in *Proc. SAE World Congr. Int. Symp. Ind. Electron. (ISIE)*, Apr. 2013, pp. 366–369.

[20] M. Farag, M. Attari, S. A. Gadsden, and S. R. Habibi, "Lithium-ion battery state of charge estimation using one state hysteresis model with nonlinear estimation strategies," *World Acad. Sci., Eng. Technol. Int. J. Mater. Metall. Eng.*, vol. 11, no. 3, pp. 237–241, Jan. 2017.

[21] Y. Ma, B. Li, G. Li, J. Zhang, and H. Chen, "A nonlinear observer approach of SoC estimation based on hysteresis model for lithium-ion battery," *IEEE/CAA J. Autom. Sinica*, vol. 4, no. 2, pp. 168–176, Apr. 2017.

[22] A. Biswas, R. Gu, P. Kollmeyer, R. Ahmed, and A. Emadi, "Simultaneous state and parameter estimation of Li-ion battery with one state hysteresis model using augmented unscented Kalman filter," in *Proc. IEEE Transp. Electrific. Conf. Expo (ITEC)*, Jun. 2018, pp. 1065–1070.

[23] T. Huria, M. Ceraolo, J. Gazzarri, and R. Jackey, "High fidelity electrical model with thermal dependence for characterization and simulation of high power lithium battery cells," in *Proc. IEEE Int. Electr. Vehicle Conf.*, Mar. 2012, pp. 4–8.

[24] G. L. Plett, "Results of temperature-dependent LiPB cell modeling for HEV SoC estimation," in *Proc. 21th Electr. Vehicle Symp. (EVS)*, Apr. 2005, pp. 1–9.

[25] J. Tian, R. Xiong, W. Shen, J. Wang, and R. Yang, "Online simultaneous identification of parameters and order of a fractional order battery model," *J. Cleaner Prod.*, vol. 247, Feb. 2020, Art. no. 119147.

[26] K. Liu, K. Li, Q. Peng, and C. Zhang, "A brief review on key technologies in the battery management system of electric vehicles," *Frontiers Mech. Eng.*, vol. 14, no. 1, pp. 47–64, Mar. 2019.

[27] S. Liu, J. Wang, Q. Liu, J. Tang, H. Liu, and Z. Fang, "Deep-discharging li-ion battery state of charge estimation using a partial adaptive forgetting factors least square method," *IEEE Access*, vol. 7, pp. 47339–47352, Apr. 2019.

[28] K. Dai, J. Wang, and H. He, "An improved SoC estimator using time-varying discrete sliding mode observer," *IEEE Access*, vol. 7, pp. 115463–115472, Aug. 2019.

[29] K. Liu, C. Zou, K. Li, and T. Wik, "Charging pattern optimization for lithium-ion batteries with an electrothermal-aging model," *IEEE Trans. Ind. Informat.*, vol. 14, no. 12, pp. 5463–5474, Dec. 2018.

[30] K. Liu, X. Hu, Z. Yang, Y. Xie, and S. Feng, "Lithium-ion battery charging management considering economic costs of electrical energy loss and battery degradation," *Energy Convers. Manage.*, vol. 195, pp. 167–179, Sep. 2019.

[31] S. Haykin, *Adaptive Filter Theory*, 4th ed. Upper Saddle River, NJ, USA: Prentice-Hall, 2002.

[32] J. Shen, S. Dusmez, and A. Khaligh, "Optimization of sizing and battery cycle life in battery/ultracapacitor hybrid energy storage systems for electric vehicle applications," *IEEE Trans. Ind. Informat.*, vol. 10, no. 4, pp. 2112–2121, Nov. 2014.

[33] X. Hu, F. Feng, K. Liu, L. Zhang, J. Xie, and B. Liu, "State estimation for advanced battery management: Key challenges and future trends," *Renew. Sustain. Energy Rev.*, vol. 114, Oct. 2019, Art. no. 109334.

[34] F. Feng, S. Teng, K. Liu, J. Xie, Y. Xie, B. Liu, and K. Li, "Co-estimation of lithium-ion battery state of charge and state of temperature based on a hybrid electrochemical-thermal-neural-network model," *J. Power Sources*, vol. 455, Apr. 2020, Art. no. 227935.

EUNSEOK CHOI received the B.S.E.E. and M.S.E.E. degrees from the Department of Electronics and Information Engineering, Korea Aerospace University, Goyang, South Korea, in 2000 and 2002, respectively, and the Ph.D. degree from the Department of Electrical and Computer Engineering, University of Seoul, Seoul, South Korea, in 2018. He is currently working at SK Holdings, Seongnam, South Korea, where he is currently a Model-based Development Engineer and a Function Leader of the Automotive Application Software Group. His current research interests include battery cell modeling, renewable energy systems, embedded vehicle systems, and real-time locating systems.

SEKCHIN CHANG received the B.S.E.E. and M.S.E.E. degrees from the Department of Electronics and Computer Engineering, Korea University, Seoul, South Korea, in 1991 and 1993, respectively, and the Ph.D. degree from the Department of Electrical and Computer Engineering, The University of Texas at Austin, Austin, TX, USA, in 2001. From 1993 to 1998, he was with the Electronics and Telecommunications Research Institute (ETRI), Daejon, South Korea. He was also with Motorola Inc., Austin, from 2000 to 2004. Since February 2004, he has been with the Department of Electrical and Computer Engineering, University of Seoul, Seoul, where he is currently a Full Professor. His current research interests include battery cell modeling, renewable energy systems, real-time embedded systems, and embedded vehicle systems.

• • •